Impact of different energies of precipitating particles on NO_x generation in the middle and upper atmosphere during geomagnetic storms.

Esa Turunen[a], Pekka T. Verronen[b], Annika Seppälä[b], Craig J. Rodger[c], Mark A. Clilverd[d], Johanna Tamminen[b], Carl-Fredrik Enell[a], Thomas Ulich[a].

[a] Sodankylä Geophysical Observatory, Tähteläntie 62, FI-99600 Sodankylä, Finland.
[b] Earth Observation, Finnish Meteorological Institute, P.O. Box 503, FI-00101 Helsinki, Finland.
[c] Department of Physics, University of Otago, P.O. Box 56, Dunedin, New Zealand.
[d] Physical Sciences Division, British Antarctic Survey (NERC), High Cross, Madingley Road, Cambridge CB3 0ET, England, U.K.

Corresponding author: Mark Clilverd email: macl@bas.ac.uk tel: +44 1223 221541 fax: +44 1223 221226

Keywords: Solar wind, geomagnetic storms, energetic precipitation, nitric oxide, ozone

Abstract: Energetic particle precipitation couples the solar wind to the Earth's atmosphere and indirectly to Earth's climate. Ionisation and dissociation increases, due to particle precipitation, create odd nitrogen (NO_x) and odd hydrogen (HO_X) in the upper atmosphere, which can affect ozone chemistry. The long-lived NO_x can be transported downwards into the stratosphere, particularly during the polar winter. Thus the impact of NO_x is determined by both the initial ionisation production, which is a function of the particle flux and energy spectrum, as well as transport rates. In this paper we use the Sodankylä Ion and Neutral Chemistry model (SIC) to simulate the production of NO_x from examples of the most realistic particle flux and energy spectra available today of solar proton events, auroral energy electrons, and relativistic electron precipitation. Large SPEs are found to produce

higher initial NO_x concentrations than long-lived REP events, which themselves produce higher initial NO_x levels than auroral electron precipitation. Only REP microburst events were found to be insignificant in terms of generating NO_x. We show that the GOMOS observations from the Arctic winter 2003-2004 are consistent with NO_x generation by a combination of SPE, auroral altitude precipitation, and long-lived REP events.

1. Introduction

Over the past few years the importance of High Speed Solar Winds Streams (HSSWS) in the solar wind has become increasingly accepted as a driver of geomagnetic activity within the Earth's magnetosphere (Friedel et al., 2002). While Coronal Mass Ejections (CMEs) are the main source of geomagnetic storms at solar maximum, the declining and minimum phase of solar activity is characterised by an increase in the occurrence rate of high-speed (>500 km/s) solar wind streams emanating from coronal holes (Richardson et al., 2001).

Although HSSWS events are not typically associated with large signatures in the D_{st} index (max >-50 nT), they do produce moderate levels of geomagnetic activity which persists for many days. In contrast CME events are more transient, driving high geomagnetic activity for typically only 1-2 days (Richardson et al., 2000). As such, the energy input to the magnetosphere during HSSWS events is comparable to or may exceed the energy input to the magnetosphere during CMEs. There are more significant electron flux enhancements in HSSWS-driven storms compared to CME-driven storms, the flux of higher-energy particles peak later in time, and many magnetospheric electromagnetic wave processes are enhanced (Hilmer et al., 2000; Vassiliadias et al., 2007). Energetic particles are ultimately lost to the atmosphere through interactions with magnetospheric waves such as chorus, plasmaspheric hiss, electromagnetic ion cyclotron waves (EMIC), and Pc5 micropulsations. The altitudes at which these particles deposit their momentum is dependent on their energy spectrum, with lower energy particles impacting the atmosphere at higher altitudes than their more energetic relatives (Rees, 1989; Rodger et al., 2007a).

Precipitating particles affect the neutral chemistry of the middle atmosphere. Direct particle impact on N_2 and ion chemical reactions produces atomic nitrogen, part of which reacts to form NO_x (Rusch et al., 1981). Additionally, ion chemistry, involving production and recombination of water cluster ions, leads to production of HO_x (Solomon et al., 1981). Both NO_x ($N+NO+NO_2$) and HO_x ($H+OH+HO_2$), although being minor gases, are important catalysts that participate in ozone loss reactions in the upper stratosphere and mesosphere, respectively (Grenfell et al., 2006). Ozone, on the other hand, affects the radiative balance, temperature, and dynamics of the atmosphere due to its capability of absorbing solar UV radiation efficiently (Brasseur and Solomon, 2005).

1.1 Solar proton events

In the upper stratosphere, larger solar proton events (SPEs) can produce order-of-magnitude changes in NO_x concentrations which, due to the long photochemical lifetime of NO_x, can last for months. Related decreases in ozone have been observed to be of the order of several tens of percent (Seppälä et al., 2004; Lopez-Puertas et al., 2005). In the presence of a strong underlying polar vortex, NO_x produced above the stratosphere in the MLT region can descend into the stratosphere (Randall et al., 2005). In 2003-2004 these conditions were highlighted by Randall et al. (2005) who reported unprecedented levels of spring-time stratospheric NO_x as a result. Rinsland et al. (2005) also observed very high NO_x mixing ratios at 40-50 km in February/March

2004 with the ACE experiment, detecting levels as high as 1365 ppbv. Seppälä et al. (2007b) showed that the NO_x descent period of 2003/04 contained 4 periods of NO_x production, beginning with in-situ stratospheric production by the solar proton events of October/November 2003, and culminating in the descent of thermospherically generated NO_x in January/February 2004. Both Siskind et al. (2000) and Seppälä et al. (2007a) showed that stratospheric NO_x concentrations at altitudes between 23-55 km were well correlated with geomagnetic activity levels (monthly average A_p).

1.2 Auroral electron precipitation

Thermospheric NO concentration is known to enhance significantly during auroral electron precipitation (Barth et al., 2001). The increase of NO in the lower thermosphere at the NO maximum is related to the relative abundances of nitrogen atoms in the ground state $N(^4S)$ and the first excited state $N(^2D)$, which is mainly produced by dissociation of N_2 by precipitating electrons, recombination of NO^+ and atomic oxygen reacting with N_2^+ ions. The first satellite observations of NO (Rusch and Barth, 1975) showed increased amounts of NO in the polar regions. Since then several studies have shown good correlation between satellite observations of thermospheric NO concentration and various indicators of auroral electron precipitation (e.g., Petrinec et al., 2003).

A significant fraction of large geomagnetic storms are associated with relativistic electron population increases in the outer radiation belt and the slot region. During storms outer radiation belt fluxes show strong drop-outs in relativistic fluxes, partially due to the D_{st} effect, and partially due to precipitation losses. The increased population decays in part through the loss, i.e., precipitation into the middle and upper atmosphere, over timescales of days to weeks driven by plasmaspheric hiss (Rodger et al., 2007b).

Even relatively mild geomagnetic disturbances increase the flux into the atmosphere of the relatively low energy electrons that are associated with the aurora (energies 1-10 keV), while large geomagnetic storms can produce relativistic electron precipitation (REP). Energetic electron precipitation from the Van Allen radiation belts occur on different timescales with differing energy ranges, driven by a wide variety of mechanisms. At this point there are still significant gaps in our understanding of the processes involved. Essentially all geomagnetic storms substantially alter the electron radiation belt populations (Reeves et al., 2003), in which precipitation losses play a major role (Green et al., 2004). A significant fraction of the energetic particles are lost into the atmosphere (Clilverd et al., 2006a), although storm-time non-adiabatic magnetic field changes also lead to losses through magnetopause shadowing (e.g., Ukhorskiy et al., 2006).

1.3 Relativistic electron precipitation

Multiple observations exist of REP on very short and relatively long time scales. For example, relativistic electron microbursts are bursty, short duration (<1 s) precipitation events containing electrons of energy >1 MeV (Imhof et al., 1992; Blake et al., 1996). Observations from the SAMPEX satellite show that REP microbursts occur at about L=4-6, and are observed predominantly in the morning sector. Primarily because of this local time dependence microbursts have been associated with very low frequency (VLF) chorus waves, although this is not consistent with the ionospheric signature of rapid REP (Rodger et al., 2007a). Estimates of flux losses due to relativistic microbursts show that they could empty the radiation belt in about a day (Lorentzen et al., 2001), and thus might produce a significant impact upon the neutral atmosphere. In contrast, precipitation events lasting minutes to hours have been observed from balloon-borne sensors (e.g., Millan et al., 2002) and subionospheric VLF measurements (Clilverd et al., 2006a). They occur at about *L*=4-7, are observed in the late afternoon/dusk sector. The observed loss rates also suggest that these minute-hour events could be the primary loss mechanism for outer zone relativistic electrons, although as with the case of REP microbursts significant assumptions are used in the loss rate estimates. It has been suggested that this precipitation may be caused by EMIC waves (Millan et al., 2002), which has been supported by EMIC observations during REP activity (Clilverd et al., 2007a).

Evidence of (thermospheric) NO being transported from auroral to lower latitudes after major geomagnetic storms is seen in 1-D modelling and observational studies based on SNOE data (Barth et al., 2003; Barth and Bailey, 2004). However, a consistent approach to latitudinal as well as vertical transport of long-lived NO_x can only be provided by 3D general circulation models. Dobbin et al. (2006) compared runs of their 3D global circulation model CMAT with and without auroral forcing, representative of auroral energy input corresponding to K_p values of 2^+ and 6^- for moderate and high activity respectively. CMAT simulations suggest that under moderate geomagnetic conditions, the most equatorward geographic latitudes to be influenced by aurorally produced NO are 30°S and 45°N. Under conditions of high geomagnetic activity, aurorally produced NO is present at latitudes poleward of 15°S and 28°N.

In this study we discuss the significance of relatively mid-energy (auroral) electron precipitation, and high-energy relativistic electron precipitation events of different durations, on the neutral atmosphere in the polar regions. This is undertaken in comparison with the effect of solar proton events. The auroral altitude electron precipitation is preferentially related to the occurrence of HSSWS in comparison with CME. Relativistic electron precipitation events are produced by large geomagnetic storms triggered by CME and HSSWS. We model the altitude and effectiveness of NO_x using the Sodankylä Ion and Neutral Chemistry model using the most realistic particle flux and energy spectra available today. We also discuss the evidence that the stratospheric polar vortex transports the precipitation-generated NO_x into the stratosphere, and how it can then affect stratospheric winds and temperatures.

2. Modelling chemistry effects of particle precipitation

Particle precipitation affects the ion-chemistry of the atmosphere. Here we particularly concentrate on the odd nitrogen (NO_x) effects, which will in turn impact ozone concentration, leading to effects on atmospheric dynamics. Figure 1 shows the reaction pathways driven by energetic particle precipitation into the stratosphere, mesosphere, and lower thermosphere. NO_x gases N, NO, and NO_2 are formed primarily in the stratosphere through the reaction $N_2O + O(^1D) \rightarrow 2NO$, and in the thermosphere through both photodissociation and photoionisation of N_2. Precipitating charged particles produce NO_x through ionisation or dissociative ionisation of N_2 and O_2 molecules, which results in the formation of N_2^+, O_2^+, N^+, O^+, and NO^+. The reactions of these ions lead to formation of both the excited nitrogen atoms $N(^2D)$ and the ground state of nitrogen $N(^4S)$ (Rusch et al., 1981; Solomon et al., 1982). Almost all of the excited nitrogen reacts with O_2 to form NO, providing a significant pathway to NO production. The NO produced is converted into NO_2 below ~65 km altitude in various reactions (see e.g. Brasseur and Solomon, 2005, pp. 336-341), but the production of NO_2 is balanced by conversion back to NO either in reaction with O, or by photolysis, the outcome of this balance giving the relative concentrations of NO and NO_2. During nighttime, when little O is available, and the above reactions are ineffective, all NO is rapidly converted to NO_2 after sunset.

The production of excess amounts of long-lived NO_x in the lower thermosphere and mesosphere can be modelled with a coupled ion-neutral chemistry model. Successful modelling of high energy particle precipitation effects during solar proton events has been recently undertaken using the Sodankylä Ion and Neutral Chemistry model, also known as SIC, which is a 1-D tool for ionosphere–atmosphere interaction studies (Turunen et al.,1996; Verronen et al., 2002). The model is readily applicable in order to accurately model the production-loss balance of NO_x, and its time development, in the cases of both auroral and relativistic electron precipitation.

The first version of the model was developed in the late 1980s to facilitate ionospheric data interpretation. A detailed description of the original SIC model, which solved the ion composition only, can be found in Turunen et al. (1996). The latest version (v. 6.9.0) solves the concentrations of 65 ions, of which 36 are positive and 29 negative, as well as 15 minor neutral species. A recent, detailed description of SIC is given by Verronen et al. (2005) and Verronen (2006). Below we briefly summarise the main details of the model. The altitude range of SIC is from 20 to 150 km, with 1-km resolution. The model includes a chemical scheme of several hundred reactions, and takes into account external forcing due to solar UV and soft X-ray radiation, electron and proton precipitation, and galactic cosmic rays. The background neutral atmosphere is generated using the MSISE-90 model (Hedin, 1991) and tables given by Shimazaki (1984). The solar flux is estimated by the SOLAR2000 model (Tobiska et al., 2000), version 2.27. The scattered component of the solar Lyman-α flux is included using the empirical approximation given by

Thomas and Bowman (1986). The model includes a vertical transport scheme, as described by Chabrillat et al. (2002), which takes into account both molecular and eddy diffusion. Within the transport code the molecular diffusion coefficients are calculated according to Banks and Kockarts (1973). The Eddy diffusion coefficient profile can be varied using the parameterisation given by Shimazaki (1971). Figure 2 shows a graphical representation of the SIC model structure, showing the inputs, dependencies, and processes with the model.

The production of NO_x in the SIC model is dependent on the particle energy spectrum, with lower energy particles ionising the atmosphere at higher altitudes than their more energetic relatives. The left panel of Figure 3 shows the ionisation rates due to a monoenergetic beam of protons with energies spanning 1-1000 MeV, in each case with a flux of 1 proton $cm^{-2}s^{-1}sr^{-1}$. The ionisation rate calculation is based on proton energy-range measurements in standard air (Bethe and Ashkin, 1953), as described in detailed by Verronen et al. (2005). These ionisation rate calculations should be contrasted with those given in the right panel, presenting the rates for monoenergetic electron beams with a flux of 100 electrons $cm^{-2}s^{-1}sr^{-1}$. The energy ranges span from 4 keV to 10 MeV, representing relatively high energy auroral electrons through to very hard REP. The electron ionisation rates make use of the expressions given by Rees (1989, chapter 3), with effective electron ranges taken from Goldberg and Jackman (1984). In the section below we use the SIC model to simulate the response of the atmosphere to different cases of energetic particle precipitation.

3. Results from SPE, auroral, and REP case studies

Here we model four separate cases of energetic particle precipitation using the SIC model to simulate the production of NO_2 using the most realistic particle flux and energy spectra available today. For each model run, we also perform a control run. We convert the precipitation energy spectra into ionisation rates as a function of altitude as discussed above, and run these through the SIC model using realistic fluxes at 70°N, 0°E in northern hemisphere winter conditions. We are then able to compare the increase in NO_x and electron number density as a result of the precipitation. The case events studied here are: an example of high levels of proton precipitation flux as seen in the Halloween storm of October 2003; pulsed auroral precipitation from Ulich et al. (2000); relativistic electron precipitation from Gaines et al. (1995) lasting several hours such as those observed by balloon experiments (Millan et al., 2002); and relativistic microbursts from Rodger et al. (2007a).

3.1 Solar proton events

The modelled response of the middle atmosphere to a solar proton event is presented in Figure 4 as an example of an event with high levels of proton precipitation. The proton flux levels are taken from the GOES-11 spectra. Electron concentrations shown in the upper panel are enhanced by several orders of magnitude during the periods of extreme forcing. This is directly dependent on the ionisation rate and thus can be used for monitoring the magnitude of the forcing below 80 km. The effects of the SPE events on 28–31 October 2003 and 3–5 November 2003 are easily identified in the upper panel of the figure as increases in electron number density at 60-100 km altitudes, particularly on 28 October, and 3 November. Once affected by proton forcing, the concentrations of NO_x ($N + NO + NO_2$) shown in the lower panel stays at an elevated level. The recovery is slow because of the long chemical lifetime of NO_x especially at high solar zenith angles (SZA, see, e.g., Brasseur and Solomon, 2005, pp. 327-358). On 26–27 October, electron number density is enhanced at 60–80 km but little change can be seen in the NO_x. However, the largest event on 28–31 October leads to enhancements of NO_x and electron number density of several hundred per cent at altitudes above 40 km. In contrast, the effect of the 3–5 November event is small on the already elevated NO_x levels. At altitudes >100 km a diurnal variation in electron number density and NO_x can be seen as part of the normal SZA-driven variability, but the SPE has little influence on it due to the energy of the protons.

3.2 Auroral electron precipitation

Figure 5 shows the modelled impact of several bursts of auroral electron precipitation on electron number density (upper panel) and NO concentration (lower panel). The electron bursts last 5 min each, starting at 23:05, 23:25, and 23:45 LT. This example is based on studies of bursty aurora of the type observed by Ulich et al. (2000). Assuming that the energy in auroral structures is deposited in monoenergetic sheets embedded within wider regions of electron precipitation with a spread of energies, we can describe the electron spectra as having a combination of Maxwellian and monoenergetic forms, where the monoenergetic component is represented typically by a Gaussian with 10% half-width. This kind of spectrum is called an 'inverted-V', and it is a common form in auroral structures with latitudinal widths between 100 m and 100 km (McFadden et al., 1990; Lanchester et al., 1998). The bursts of electrons have a characteristic energy of 5 keV and a total energy flux of 10 mW m^{-2}, of which 75% is in the monoenergetic component and 25% in the Maxwellian component. A large fraction of the total energy is deposited at altitudes around 110 km by the monoenergetic part, while the Maxwellian part, which has a wide energy distribution, affects altitudes above 85 km.

The response of electron number density to the precipitation of energetic electrons is immediate. The effect is largest at around 110 km altitude, where the density increases by nearly two orders of magnitude. After the first precipitation burst, the electron number density decreases exponentially reaching, after 15 min, a level about one order-of-magnitude larger than the background level prior to the burst. The second and third burst repeats this behaviour in much the same way. After the third burst, electron number densities decrease to values within about 50% of the background after some 2 hours. Between 05:00 and 06:00 LT the Sun begins to rise and solar radiation ionises the atmosphere.

Like the electron number density, the NO concentration shown in the lower panel of Figure 5 responds immediately to the precipitation, increasing by a factor of about 1.35 at 115 km, where the relative effect is most pronounced. However, while the electron number density decreases rapidly after the bursts, the NO concentration decreases by only about 10% during the 15 min before the next burst. The second burst causes the NO concentration to increase by a factor of 1.3 from the already elevated level. After an intermediate decrease of 15% or so, the third burst brings about another increase by a factor of about 1.25. Thus there is a cumulative effect of the subsequent electron precipitation bursts on the NO concentration, which is gradually 'pumped up' to about 1.75 times the background level during the third burst. Thereafter it settles after some 2 hours at about 1.65 times the background and remains fairly constant during the rest of the night. After sunrise the NO concentration begins to decrease slowly, and at noon on the following day it is still about 1.25 times higher than that of the control run. The amount of NO produced depends on the total energy input, which is a product of the energy flux and the duration of the precipitation. Fifteen minutes of bursts with 10 mW m^{-2} flux results in a total energy input per unit area of 9.0 J m^{-2}, which is a moderate input compared to some other studies (e.g., Barth et al., 2001), who applied a total energy of 64.8 J m^{-2}.

3.3 Relativistic electron precipitation

The ionospheric (upper panel) and atmospheric (lower panel) response for long-lasting REP is shown in Figure 6, following the same format as Figure 5. The REP is estimated using the precipitating fluxes measured in the bounce loss cone at *L*=3.5-4 by the UARS on 18 May 1992 (Gaines et al., 1995). We use this precipitation measurement to provide an indicative example of long-lasting REP, while noting that the significant unknowns at this stage as to the spectrum and fluxes for typical events. The spectrum of this REP event is very hard, containing significant fluxes at energies as high as 5 MeV (Gaines et al., Fig. 3, 1995). Ionisation rates calculated for this REP event using the approach outlined in section 2 lead to increased atmospheric ionisation rates at altitudes as low as ~30-40 km, peaking at ~60 km. The atmospheric impact is then determined by combining these ionisation rates with the SIC model assuming a 3-hour continuous precipitation process. In the upper panel an increase in electron number density can be seen at 50–100 km starting at 12 LT and ending as the REP forcing is turned off at 15 LT. In the lower panel, the NO increases steadily from 12-15 LT, peaking at altitude of 60-80 km with a 3 order of magnitude increase over background levels. Unlike the electron number density changes the NO is long-lived following the end of the REP forcing.

3.4 REP microbursts

In order to estimate the atmospheric impact of REP microbursts we assume a 0.1 s burst of 2 MeV monoenergetic relativistic electrons with a REP flux of 100 el.cm^{-2}s^{-1}sr^{-1} taken from the results of Rodger et al. (2007a), who found that such a burst produced reasonable agreement with short bursts of relativistic electron precipitation, detected by a subionospheric propagation sensor in Sodankylä, Finland. The results from SIC are shown in Figure 7. The REP microburst was applied to the SIC model at 0.5 s and the effect can been clearly seen in the electron number density plot in the upper panel. At altitudes of 50 km the enhanced electron number density recovers in ~1 s, while at altitudes of ~70 km the recovery takes ~30 s. No substantial enhancement of NO can be seen in the lower panel. In fact, the NO enhancements are too close to the numerical noise level of the modelling for us to have confidence in the values. Thus multiple forcing events have not been applied to the model study as each and every event produces results too noisy to be trusted. However, the observed repetition rate for microbursts from ground-based measurements is too low for the accumulation to become significant. A similar insignificant NO_x enhancement was found for the considerably softer lightning-generated whistler induced electron precipitation, were >4000 precipitation bursts occurred over ~8 hours (Rodger et al., 2007c).

4. Descent of NOx to the stratosphere via the polar vortex

Our case studies using the SIC model have shown that SPEs, auroral altitude electron precipitation, and long-lived REP events produce mesospheric and thermospheric NO_x that is long-lived in polar regions during the winter. In this section we discuss how the NO_x can be transported vertically downwards into the stratosphere and how, once it has arrived, it can influence ozone chemistry and the radiative balance of the lower atmosphere. The balance between the occurrence of descending air during strong polar vortex conditions and the occurrence of significant levels of NO_x generated by energetic precipitation events is fundamental to the delivery of high altitude NO_x into the polar stratosphere. The following section uses the SIC model predictions of NO_x production by SPEs, auroral precipitation, and REP to identify mechanisms operating during the Arctic winter 2003-2004.

The air inside the polar vortex is effectively isolated from lower-latitude air. In the southern hemisphere the polar vortex is generally stable during the entire winter due to the relatively flat topography and the distribution of sea and land around the pole of the Southern hemisphere. The Northern polar vortex is less stable because of wave patterns disturbed by mountain ranges such as the Himalayas with a large interannual variability in its stability (Brasseur and Solomon, 2005, Chapter 6).

In the winter polar middle atmosphere transport is largely determined by the polar vortex. In the winter pole, near the polar night terminator, strong temperature gradients lead to formation of the Polar Night Jet (PNJ). As shown in Figure 8a, the PNJ is a strong eastward (westerly) wind in the upper stratosphere-lower mesosphere near 60° N/S latitude, formed due to the thermal wind balance (Solomon, 1999; Holton, 2004). The winds in the PNJ, which reach their peak of about 80 m/s near 60 km altitude, act as a transport barrier between polar and mid-latitude air, blocking meridional transport and isolating the air in the polar stratosphere and thus forming outer edge of the so-called polar vortex. The edge of the winter polar vortex is usually near 60° N/S and it extends from approximately 16 km to the mesosphere.

The isolation is greater, and the polar vortex more stable, in the Antarctic where there is less planetary wave activity affecting the vortex than in the Arctic. In the Arctic, the atmospheric wave activity disturbs the vortex, leading to greater mixing and faster downward motion, compared with those in the Antarctic vortex (Solomon, 1999). The approximate location of the PNJ is presented in Figure 8a and the approximate location of the edge of the polar vortex in Figure 8b.

The large-scale meridional circulation in the stratosphere is determined by the Brewer-Dobson circulation. The Brewer-Dobson circulation is formed by rising motion from the troposphere to the stratosphere in the tropics, poleward transport at stratospheric altitudes and sinking motion at mid- and high latitudes (Solomon, 1999). In the mesosphere, the meridional circulation is formed by a single cell in which rising motion takes place in the summer pole starting from the stratosphere, pole-to-pole transport in mesosphere-lower-thermosphere, and downward motion in the winter pole mesosphere, down to the stratosphere. Horizontal transport in the stratosphere and mesosphere is determined by winds in the zonal (longitudinal, u) and meridional (latitudinal, v) directions as presented in Figure 8a. In the polar winter stratosphere the mean zonal winds are in general directed eastwards (westerlies) along with the PNJ. At higher altitudes the zonal winds remain westerly up to about 90 km altitude above which the wind direction is reversed (Brasseur and Solomon, 2005).

Inside the polar vortex the vertical descent rate varies from year to year, and also with respect to the distance from the vortex edge, as well as with altitude (Manney et al., 1994; Rosenfield and Schoeberl, 2001). Callaghan and Salby (2002) have shown from model simulations that, in general, the maximum descent rates (2 mm/s, ~5 km/month) in the wintertime Northern Hemisphere (NH) middle and upper stratosphere are found near 60° latitude. At lower altitudes the descent is slower, with vertical descent rates of 0.4-0.7 mm/s in the Antarctic middle stratosphere (Kawamoto and Shiotani, 2000). In the mesosphere the downwelling rates increase to several mm per second (Callaghan and Salby, 2002) this being due to due to the cooling rates increasing with altitude (Rosenfield et al., 1994). In the NH, where the polar vortex is more disturbed than in the SH, there is more year to year variation in the descent, as changes in the wave activity and frequently occurring stratospheric warmings affect the vortex conditions (Rosenfield and Schoeberl, 2001; Brasseur and Solomon, 2005).

4.2 Arctic winter 2003-2004

Figure 9 presents observed effects of energetic particle precipitation on the NO_x levels and the descent of the NO_x to lower altitudes during the Arctic winter 2003-2004 taken from Seppälä et al. (2007b). The top panel of the figure shows the GOES-measured proton flux of protons with energy >10 MeV together with the geomagnetic activity index K_p. The middle panel shows a radio wave ionisation index which indicates enhanced ionisation levels inside the 70-90 km altitude range (Clilverd et al., 2007b), measured through the analysis of radio wave propagation conditions between Iceland and Svalbard. The lower panel presents NO_2 mixing ratios from two satellite instruments complementing each other. The first of the instruments is GOMOS (Global Ozone Monitoring by Occultation of Stars) flying on board the Envisat satellite (Kyrölä et al., 2004). The instrument measures, among others, nighttime ozone and NO_2 vertical profiles in the middle atmosphere (with NO_2 vertical resolution of 4 km in the upper stratosphere and mesosphere). The second instrument is the POAM III (Polar Ozone and Aerosol Measurement) carried on the SPOT-4 satellite, measuring tropospheric and stratospheric daytime ozone, NO_2 (with vertical resolution of < 2 km below 40 km) as well as other minor gases (Lucke et al., 1999). In the lower panel of Figure 9 GOMOS nighttime NO_2 mixing ratios are shown to illustrate the amount of NO_x in the altitude range 30-70 km in the 65-85°

latitude range (nighttime NO_2 is a good representation of the total $NO_x = NO + NO_2$ in stratosphere-lower mesosphere region, see section 2). To follow the descent of NO_x beyond the polar night (beyond Feb 2004) the daytime NO_2 measurements are shown below the 45 km altitude. Note that the difference in magnitudes between the GOMOS and POAM III observations is due to the diurnal variation of NO_2. The radio wave ionisation index shown in the 70-90 km region in Figure 9 indicates that during the winter there were two principal periods showing significant ionisation increases at ~80 km, either created in-situ by particle precipitation or by the ionisation of NO_x by Lyman-α as the NO_x descends from higher altitudes (Seppälä et al., 2007b; Clilverd et al., 2007b).

The first period of NO_x production (labelled **1** in Figure 9) occurred during the Halloween storm at the end of October 2003, and can be strongly associated with solar proton precipitation during the storm. Our modelling results presented in this study shows consistency with the GOMOS observations shown in that significant concentrations of NO_x are generated at altitudes of 50-60 km. NO_x descent driven by the polar vortex continues after the end of the SPEs, and transports the NO_x to lower altitudes. The descent of the NO_x enhancement appears to take about 1 month to reach 40 km altitude, and the final NO_x levels are about 3 times larger than normal (Jackman et al., 2005).

Following the initial NO_x enhancement a second period of enhanced NO_x is observed from mid-November to mid-December (labelled **2**). This appears to descend as well, at approximately the same rate as the first enhancement, but only reaches lower altitudes of 45-50 km before disappearing at all altitudes due to the reconfiguration of the polar vortex at this time (Randall et al., 2005). During this period there were two small solar proton events, and several large geomagnetic storms, which could have generated some NO_x at altitudes >60 km, but the timing and altitude range are consistent with simulation (Semeniuk et al., 2005) where enhanced thermospheric ionisation by low energy electrons was included from the Halloween storm and moderately disturbed periods consistent with HSSWS shortly afterward. Our model simulations of auroral electron precipitation production of NOX at high altitudes (110-120 km in Figure 5) are consistent with this picture.

A third period of NO_x enhancement starts on 12/13 January 2004 (labelled **3**), and is not associated with any particular storm, but rather with the strengthening of the polar vortex in the upper stratosphere as indicated by cold zonal mean temperatures at 2mB (http://www.cpc.ncep.noaa.gov/products/stratosphere) and consequent strong downward vertical transport from thermospheric altitudes. Between mid-December and early January no significant traces of NO_x are observed at any altitude. The NO_x observed at the start of period 3 shows no sign of been generated at 50-60 km as with SPEs, nor does it appear to be created at 60-70 km as with REP. The lack of any geomagnetic storms at the time is consistent with this view. From our model predictions we determine that the most likely source of the NO_x is auroral altitudes (>70 km), although the high concentrations of NO_x suggest a significant period of generation rather than bursts of aurora.

The enhancement is first observed at high altitudes and can be followed in each instruments dataset in turn until the enhancement reaches the upper stratosphere in April 2004. No single geomagnetic storm or solar proton event can be identified as the source of this NO_x, and the production altitude is reported to be >70 km (Clilverd et al., 2007b), i.e., consistent with an auroral altitude source as modelled in Figure 5. The onset date is consistent with the start of strong downward vertical transport in the polar vortex as the upper stratospheric vortex re-strengthens (see http://www.cpc.ncep.noaa.gov/products/stratosphere) following a stratospheric warming period at the end of December (Clilverd et al., 2006b). The amount of NO_x in this third event is 4 times the background levels once it reaches 40 km, and is significantly longer-lived than the previous two enhancements (4 months compared with 1 month). During the descent period of the third enhancement a secondary enhancement of NO_x can be seen in mid-February 2004 at all altitudes above about 55 km (labelled **4**). The timing of this NO_x increase is coincident with a large geomagnetic storm that occurred on 11 February 2004, which had no associated solar proton event. The NO_x enhancements are significant, and add to the already descending NO_x at 50-55 km, but disappear at higher altitudes after about one week. From our model prediction we find that this secondary enhancement is clearly the result of REP generating NO_x at altitudes of about 55-70 km, i.e., electron energies of 200-1000 keV, as shown in our modelling study in Figure 6.

From the analysis of the observations shown in Figure 9 we can determine that all three NO_x generation mechanisms took place during the Arctic winter 2003-2004. Due to the long lifetime of NO_x in the dark polar winter the NO_x accumulated at altitudes of 50-90 km in the early winter because of SPEs and auroral electron precipitation, and also accumulated in the late winter because of auroral electron precipitation and REP.

4.3 The ozone balance of the stratosphere

Descending NO_x enhancements from energetic particle precipitation changes the ozone balance of the stratosphere. Since ozone is an important source of heating in the stratosphere, reductions in ozone would be expected to lead to cooling of the stratosphere. By including an experimentally based energetic electron precipitation

NO_y production (EEP-NO_y) into a Chemistry-Climate model, Rozanov et al. (2005) were able to identify a 2 K cooling in the polar middle atmosphere at high latitudes (0.5 K cooling at tropical latitudes) compared with a simulation which did not include the EEP-NO_y source. Their model results also showed detectable changes (from -1 K to +2.4 K) in the surface air temperatures in the northern polar region. These were a result of about a 30% decrease in ozone at high polar latitudes within the polar vortex, the ozone decrease outside the vortex being around 3-5%. The model study of Rozanov et al. (2005) was based on a one year simulation, 15 years of observations reported by Sinnhuber et al. (2006) also suggest that there is a relation between energetic electron precipitation (GOES observed electron fluxes) and middle stratospheric ozone observed from ozone soundings in the Arctic. Langematz et al. (2005) have included a REP-NO_x source in a 11-year solar cycle simulation. Their results, like Rozanov et al. (2005), suggest that the NO_x source by particles and its transport from the mesosphere to the stratosphere in the polar vortex are important for stratospheric O_3. We have shown here that the source of NO_x by particles are a combination of three mechanisms, suggesting more complex variability than in the reported modelling studies above, but all are associated with solar and geomagnetic activity cycles. Detailed estimates, of the influence on stratospheric temperatures, due to each of these three mechanisms will be undertaken in future work.

5. Summary

In this study we have discussed the significance of solar proton events, relatively low-energy (auroral altitude) electron precipitation, and high-energy relativistic electron precipitation events of different durations, on the neutral atmosphere in the polar regions. The auroral altitude electron precipitation is preferentially generated by HSSWS in comparison with CME events. In contrast, both CME and HSSWS-triggered geomagnetic storms are likely to produce relativistic electron precipitation events. We have predicted the altitude and effectiveness of NO_x generation at 70°N, 0°E in northern hemisphere winter conditions using the Sodankylä Ion and Neutral Chemistry model (SIC), imposing the most realistic particle flux and energy spectra available in the literature at the time of writing. Large SPEs are found to produce higher initial NO_x concentrations than long-lived REP events, which themselves produce higher initial NO_x levels than auroral electron precipitation. Only REP microburst events were found to be insignificant in terms of generating NO_x.

We also analysed the observed effects of energetic particle precipitation on the NO_x levels and the descent of the NO_x to lower altitudes during the Arctic winter 2003-2004 as shown by Seppälä et al. (2007b), and discuss them in terms of the case studies modelled using SIC in this paper. We show that the GOMOS observations from the Arctic winter 2003-2004 are consistent with NO_x generation by a combination of SPE, auroral altitude precipitation, and long-lived REP events. Each NO_x generation mechanism occurred independently during the winter, but the long-lived NO_x eventually accumulated, and in the presence of a strong polar vortex lead to levels of NO_x in the stratosphere that could produce stratospheric wind and temperature changes that are consistent with previously published results.

Acknowledgements. The work of the CHAMOS team (Chemical Aeronomy in the Mesosphere and Ozone in the Stratosphere, http://www.sgo.fi/chamos/) during 2002-2007 has been supported by the Academy of Finland.

References

Banks, P. M., Kockarts G., 1973. Aeronomy, vol. B, chap. 15, Elsevier, New York.

Barth, C. A., Baker D. N., Mankoff K. D., 2001. The northern auroral region as observed in nitric oxide, Geophys. Res. Lett., 28, 1463-1466.

Barth, C. A., Mankoff K. D., Bailey S. M., Solomon S. C., 2003. Global observations of nitric oxide in the thermosphere, J. Geophys. Res., 108, 1027, doi:10.1029/2002JA009458.

Barth C. A., Bailey S. M., 2004. Comparison of a thermospheric photochemical model with Student Nitric Oxide Explorer (SNOE) observations of nitric oxide, J. Geophys. Res., 109, A03304, doi:10.1029/2003JA010227.

Bethe, A. H., Ashkin J., 1953. Passage of radiations through matter, in Experimental Nuclear Physics, vol. 1, edited by E. Segre, pp. 166– 251, John Wiley, Hoboken, N. J.

Blake, J. B., Looper M. D., Baker D. N., Nakamura R., Klecker B., Hovestadt D., 1996. New high temporal and spatial resolution measurements by SAMPEX of the precipitation of relativistic electrons, Adv. Space Res., 18(8), 171-186.

Brasseur, G. P., Solomon S., 2005. Aeronomy of the Middle Atmosphere, 3rd revised and enlarged ed., Springer, Dordrecht.

Callaghan, P. F., Salby M. L., 2002. Three-Dimensionality and Forcing of the Brewer-Dobson Circulation, Journal of the Atmospheric Sciences, 59, 976–991.

Chabrillat, S., Kockarts G., Fonteyn D., Brasseur G., 2002. Impact of molecular diffusion on the CO2 distribution and the temperature in the mesosphere, Geophys. Res. Lett., 29(15), 1729, doi:10.1029/2002GL015309.

Clilverd, M. A., Rodger C. J., Ulich Th., 2006a. The importance of atmospheric precipitation in storm-time relativistic electron flux drop outs, Geophys. Res. Lett., 33, L01102, doi:10.1029/2005GL02466.

Clilverd, M.A., Seppälä A., Rodger C. J., Verronen P. T., Thomson N. R., 2006b. Ionospheric evidence of thermosphere-to-stratosphere descent of polar NO_x, Geophysical Research Letters, 33, L19811, doi:10.1029/2006GL026727.

Clilverd, M. A., Rodger C. J., Millan R. M., Sample J. G., Kokorowski M., McCarthy M. P., Ulich Th., Raita T., Kavanagh A. J., Spanswick E., 2007a. Energetic particle precipitation into the middle atmosphere triggered by a coronal mass ejection, J. Geophys. Res., 112, A12206, doi:10.1029/2007JA012395.

Clilverd, M. A., Seppälä A., Rodger C. J., Thomson N. R., Lichtenberger J., and Steinbach P., 2007b. Temporal variability of the descent of high-altitude NO_X inferred from ionospheric data, J. Geophys. Res., 112, A09307, doi:10.1029/2006JA012085.

Dobbin, A. L., Aylward A. D., Harris M. J., 2006. Three-dimensional GCM modeling of nitric oxide in the lower thermosphere, J. Geophys. Res., 111, A07314, doi:10.1029/2005JA011543.

Friedel, R. H. W., Reeves G. D., Obara T., 2002. Relativistic electron dynamics in the inner magnetosphere - a review, J. Atmos. Solar-Terr. Phys., 64 (2), 265-282.

Gaines, E. E., Chenette D. L., Imhof W. L., Jackman C. H., Winningham J. D., 1995. Relativistic electron fluxes in May 1992 and their effect on the middle atmosphere, J. Geophys. Res., 100(D1), 1027–1034.

Goldberg, R. A., Jackman C. H., 1984. Nighttime auroral energy deposition in the middle atmosphere, J. Geophys. Res., 89, A7, 5581-5596.

Green, J. C., Onsager T. G., O'Brien T. P., Baker D. N., 2004. Testing loss mechanisms capable of rapidly depleting relativistic electron flux in the Earth's outer radiation belt, J. Geophys. Res., 109, A12211, doi:10.1029/2004JA010579.

Grenfell, J. L., Lehmann R., Mieth P., Langematz U., Steil B., 2006. Chemical reaction pathways affecting stratospheric and mesospheric ozone, J. Geophys. Res., 111, D17311, doi:10.1029/2004JD005713.

Hedin, A. E., 1991. Extension of the MSIS thermospheric model into the middle and lower atmosphere, J. Geophys. Res., 96, 1159– 1172.

Hilmer, R. V., Ginet G. P., Cayton T. E., 2000. Enhancement of equatorial energetic electron fluxes near L=4.2 as a result of high speed solar wind streams. J. Geophys. Res., 105 (A10), 23311-23322.

Holton, J. R., 2004. An Introduction to Dynamic Meteorology, 4th ed., Elsevier Academic Press, ISBN: 0-12-354016-X.

Imhof, W. L., Voss H. D., Mobilia J., Datlowe D. W., Gaines E. E., McGlennon J. P., Inan U. S., 1992. Relativistic electron microbursts, J. Geophys. Res., 97, 13829-13837.

Jackman, C. H., DeLand M. T., Labow G. J., Fleming E. L., Weisenstein D. K., Ko M. K. W., Sinnhuber M., Russell J. M., 2005. Neutral atmospheric influences of the solar proton events in October-November 2003, J. Geophys. Res., 110, A09S27, doi:10.1029/2004JA010888.

Kawamoto, N., Shiotani M., 2000. Interannual variability of the vertical descent rate in the Antarctic polar vortex, J. Geophys. Res., 105, 11,935–11,946, doi:10.1029/2000JD900076.

Kyrölä, E., et al., 2004. GOMOS on Envisat: An overview, Adv. Space Res., 33, 1020-1028.

Lanchester, B. S., Rees M. H., Sedgemore K. J. F., Palmer J. R., Frey H. U., Kaila K. U., 1998. Ionospheric response to variable electric fields in small-scale auroral structures, Ann. Geophys., 16, 1343-1354.

Langematz, U., J. L. Grenfell, K. Matthes, P. Mieth, M. Kunze, B. Steil, C. Bruhl, 2005. Chemical effects in 11-year solar cycle simulations with the Freie Universität Berlin Climate Middle Atmosphere Model with online chemistry (FUB-CMAM-CHEM), Geophys. Res. Lett., 32, L13803, doi:10.1029/2005GL022686.

Lopez-Puertas, M., Funke B., Gil-Lopez S., von Clarmann T., Stiller G. P., Hopfner M., Kellman S., Fischer H., Jackman C. H., 2005. Observation of NO_X enhancements and ozone depletion in the northern and southern hemispheres after the October-November 2003 solar proton events, J. Geophys. Res., 110 (A9), doi:10.1029/2005JA011050.

Lorentzen, K. R., Looper M. D., Blake J. B., 2001. Relativistic electron microbursts during the GEM storms, Geophys. Res. Lett. 28 (13), p. 2573 doi: 10.1029/2001GL012926.

Lucke, R. L., et al., 1999. The Polar Ozone and Aerosol Measurement (POAM) III instrument and early validation results, J. Geophys. Res., 104(D15), 18,785–18,800.

Manney, G. L., Zurek R. W., O'Neill A., Swinbank R., 1994. On the Motion of Air through the Stratospheric Polar Vortex., Journal of the Atmospheric Sciences, 51, 2973–2994.

McFadden, J P., Carlson C. W., Boehm M. H., 1990. Structure of an energetic narrow discrete arc, J. Geophys. Res., 95, 6533-6547.

Millan, R. M., Lin R. P., Smith D. M., Lorentzen K. R., McCarthy M. P., 2002. X-ray observations of MeV electron precipitation with a balloon-borne germanium spectrometer, Geophys. Res. Lett., 29(24), 2194, doi:10.1029/2002GL015922.

Petrinec, S. M., Imhof W. L., Barth C. A., Mankoff K. D., Baker D. N., Luhmann J. G., 2003. Comparisons of thermospheric high-latitude nitric oxide observations from SNOE and global auroral X-ray bremsstrahlung observations from PIXIE, J. Geophys. Res., 108 (A3), 1123, doi:10.1029/2002JA009451.

Randall, C.E., et al., 2005. Stratospheric effects of energetic particle precipitation in 2003-2004, Geophys. Res. Lett., 32 (5), L05802, doi:10.1029/2004GL022003

Rees, M. H., 1989. Physics and chemistry of the upper atmosphere, Cambridge University Press, Cambridge.

Reeves, G.D., et al., 2003. Acceleration and loss of relativistic electrons during geomagnetic storms, Geophys. Res. Lett, vol. 30(10), 1529, doi:10.1029/2002GL016513.

Richardson, I. G., Cliver E. W., Cane H. V., 2000. Sources of geomagnetic activity over the solar cycle: Relative importance of coronal mass ejections, high-speed streams, and slow solar wind. J. Geophys. Res., 105 (A8), 18203-18213.

Richardson, I. G., Cliver E. W., Cane H. V., 2001. Sources of geomagnetic storms for solar minimum and maximum conditions during 1972-2000. Geophys. Res. Lett., 28 (13), 2569-2572 .

Rinsland, C. P., Boone C., Nassar R., Walker K., Bernath P., McConnell J. C., Chiou L., 2005. Atmospheric Chemistry Experiment (ACE) Arctic stratospheric measurements of NO_X during February and March 2004: Impact of intense solar flares, Geophys. Res. Lett., 32, L16S05, doi:10.1029/2005GL022425.

Rodger, C. J., Clilverd M. A., Nunn D., Verronen P. T., Bortnik J., Turunen E., 2007a. Storm-time short-lived bursts of relativistic electron precipitation detected by subionospheric radio wave propagation, J. Geophys. Res., 112, A07301, doi:10.1029/2007JA012347.

Rodger, C. J., Clilverd M. A., Thomson N. R., Gamble R. J., Seppälä A., Turunen E., Meredith N. P., Parrot M., Sauvaud J. A., Berthelier J.-J., 2007b. Radiation belt electron precipitation into the atmosphere: recovery from a geomagnetic storm, J. Geophys. Res., 112, A11307, doi:10.1029/2007JA012383.

Rodger, C. J., Enell C.-F., Turunen E., Clilverd M. A., Thomson N. R., Verronen P. T., 2007c. Lightning-driven inner radiation belt energy deposition into the atmosphere: Implications for ionisation-levels and neutral chemistry, Annales Geophys., 25, 1745-1757.

Rosenfield, J. E., Schoeberl M. R., 2001. On the origin of polar vortex air, Journal of Geophysical Research, 106, 33,485–33,498, doi:10.1029/2001JD000365.

Rosenfield, J. E., Newman P. A., Schoeberl M. R., 1994. Computations of diabatic descent in the stratospheric polar vortex, Journal of Geophysical Research, 99, 16,677.

Rozanov, E., Callis L., Schlesinger M., Yang F., Andronova N., Zubov V., 2005. Atmospheric response to NO_y source due to energetic electron precipitation, Geophysical Research Letters, 32 (14).

Rusch, D. W., Barth C. A., 1975. Satellite measurements of nitric oxide in the polar region, Journal of Geophysical Research, 80, 3719–3721.

Rusch, D. W., Gerard J.-C., Solomon S., Crutzen P. J., Reid G. C., 1981. The effect of particle precipitation events on the neutral and ion chemistry of the middle atmosphere - I. Odd nitrogen, Planet. Space Sci., 29, 767-774.

Salby, M. L., 1996. Fundamentals of Atmospheric Physics. International Geophysics series, Volume 61. Academic Press Inc., San Diego, ISBN: 978-0-12-615160-2.

Semeniuk, K., McConnell J. C., Jackman C. H., 2005. Simulation of the October-November 2003 solar proton events in the CMAM GCM: Comparison with observations, Geophysical Research Letters, 32, L15S02, doi:10.1029/2005GL022392.

Seppälä, A., Observations of production and transport of NO_x formed by energetic particle precipitation in the polar night atmosphere, 2007. PhD thesis, Finnish Meteorological Institute Contributions No. 62, ISBN 978-952-10-4181-5 (pdf), Yliopistopaino Helsinki.

Seppälä, A., Verronen P T., Kyrölä E., Hassinen S., Backman L., Hauchecorne A., Bertaux J. L., Fussen D., 2004. Solar Proton Events of October-November 2003: Ozone depletion in the Northern hemisphere polar winter as seen by GOMOS/Envisat, Geophys. Res. Lett., 31, L19,107, doi:10.1029/2004GL021042.

Seppälä, A., Verronen P. T., Clilverd M. A., Randall C. E., Tamminen J., Sofieva V., Backman L., Kyrölä E., 2007a. Arctic and Antarctic polar winter NO_x and energetic particle precipitation in 2002-2006, Geophys. Res. Lett., Vol. 34, No. 12, L12810, doi: 10.1029/2007GL029733.

Seppälä, A., M. A. Clilverd, and C. J. Rodger, 2007b. NO_x enhancements in the middle atmosphere during 2003-2004 polar winter: The relative significance of Solar Proton Events and the Aurora as a source. J. Geophys. Res., 112, D23303, doi:10.1029/2006JD008326.

Sinnhuber, B.-M., von der Gathen, P., Sinnhuber, M., Rex, M., K., Langlo, G., Oltmans, S. J., 2006. Large decadal scale changes of polar ozone suggest solar influence, Atmos. Chem. Phys., 6, 1835-1841, 2006.

Shimazaki, T.,1971. Effective eddy diffusion coefficient and atmospheric composition in the lower thermosphere. J. Atmos. Terr. Phys. 33 (1971), pp. 1383–1401.

Shimazaki, T. 1984. Minor Constituents in the Middle Atmosphere (Developments in Earth and Planetary Physics, No 6), D. Reidel Publishing Co., Dordrecht, Holland.

Siskind, D.E., Nedoluha G. E, Randall C. E, Fromm M., Russell J. M., 2000. An assessment of Southern Hemisphere stratospheric NO_x enhancements due to transport from the upper atmosphere, Geophysical Research Letters, 27 (3), 329-332.

Solomon, S., 1999. Stratospheric ozone depletion: a review of concepts and history, Reviews of Geophysics, 37(3), 275–316.

Solomon, S., Rusch D. W., Gerard J.-C., Reid G. C., Crutzen P. J., 1981. The effect of particle precipitation events on the neutral and ion chemistry of the middle atmosphere: II. Odd hydrogen, Planet. Space Sci., 8, 885-893.

Solomon, S., Crutzen P. J., Roble R. G., 1982a. Photochemical coupling between the thermosphere and the lower atmosphere .1, Odd nitrogen from 50 to 120 km, J. Geophys. Res., 87, 7206-7220.

Solomon, S., Reid G. C., Roble R. G., Crutzen P. J., 1982b. Photochemical coupling between the thermosphere and the lower atmosphere .2, D-region ion chemistry and the winter anomaly, J. Geophys. Res., 87, 7221-7227.

Thomas, L., Bowman M. R., 1986. A study of pre-sunrise changes in negative ions and electrons in the D-region, J. Atmos. Terr. Phys., 4, 219.

Tobiska, W. K., Woods T., Eparvier F., Viereck R., Floyd L. D. B., Rottman G., White O. R., 2000. The SOLAR2000 empirical solar irradiance model and forecast tool, J. Atmos. Sol. Terr. Phys., 62, 1233–1250.

Turunen, E., Matveinen H., Tolvanen J., Ranta., 1996. D-region ion chemistry model, in STEP Handbook of Ionospheric Models, edited by R. W. Schunk, pp. 1-25, SCOSTEP Secretariat, Boulder, Colorado, USA.

Ukhorskiy A. Y., Anderson B. J., Brandt P. C., Tsyganenko N. A., 2006. Storm time evolution of the outer radiation belt: Transport and losses, J. Geophys. Res., 111, A11S03, doi:10.1029/2006JA011690.

Ulich, Th., Turunen E., Nygrén T., 2000. The Effective Recombination Coefficient in the Lower Ionosphere During Localised Precipitation of Auroral Electrons, Adv. Space Res., 25, 47-50.

Vassiliadis, D., Mann I. R., Fung S. F., Shao, X., 2007. Ground Pc3-Pc5 wave power distribution and response to solar wind velocity variations. Planet. Space Sci., 55 (6), 743-754.

Verronen, P. T., Turunen E, Ulich T., Kyrölä E., 2002. Modelling the effects of the October 1989 solar proton event on mesospheric odd nitrogen using a detailed ion and neutral chemistry model, Annales Geophysicæ, 20, 1967–1976.

Verronen, P. T., Seppälä A., Clilverd M. A., Rodger C. J., Kyrölä E., Enell C. F., Ulich T., Turunen E., 2005. Diurnal variation of ozone depletion during the October-November 2003 solar proton event, *J. Geophys. Res.*, Vol. 110, No. A9, doi:10.1029/2004JA010932.

Verronen, P. T., Ionosphere-atmosphere interaction during solar proton events, 2006. Ph. D thesis, Finnish Meteorological Institute Contributions No. 55, ISBN 952.10.3111.5 (pdf), Yliopistopaino Helsinki.

Figure Captions:

Figure 1. Particle precipitation effects on the ion-chemistry of the atmosphere.

Figure 2. Schematic structure of the Sodankylä Ion and Neutral Chemistry model. The circles, tilted squares, and squares indicate external input, external models used, and modules of the SIC model, respectively (taken from Verronen, Fig 4.1, 2006).

Figure 3. Altitude versus ionisation rates for monoenergetic beams of protons 1-1000 MeV (left) and electrons 4-4000 keV (right).

Figure 4. The effect of the Halloween solar proton events on electron number density and NO_x as modelled by SIC at 70° N latitude, 0° longitude. The simulated electron number density (log(m^{-3})), from 40-120 km altitude, with time is shown in the upper panel, and the concentration of NO_x (log(m^{-3})) over the same altitude range is shown in the lower panel. Maximum NO_x production occurs at ~50 km altitudes.

Figure 5. The effect of auroral electron bursts on electron number density and NO concentration. The bursts of electrons have a characteristic energy of 5 keV and a total energy flux of 10 mW m^{-2}. Upper panel: electron number density during the burst run. Lower panel: the behaviour of NO concentration relative to the background level, i.e., the result of the burst run divided by the result of the control run. The electron bursts last 5 min each, starting at 23:05, 23:25, and 23:45 LT.

Figure 6. Same as Figure 5, but showing the effect of a 3 hour long burst of REP on electron number density and NO_x levels using the precipitating fluxes measured in the bounce loss cone at L=3.5-4 by the UARS on 18 May 1992 (Gaines et al., 1995). The spectrum of the REP event is very hard, containing significant fluxes at energies as high as 5 MeV.

Figure 7. Same as Figure 5, but showing the effect of a REP microburst on electron number density and NO_x levels. We have assumed a 0.1 s burst of 2 MeV monoenergetic relativistic electrons with a flux taken from those reported by SAMPEX.

Figure 8a: Approximate location of the Northern Hemisphere Polar Night Jet, inside which the polar vortex is formed, and the wind vector directions (zonal u, meridional v and vertical w). – **8b**: Different phenomena in the winter pole middle atmosphere. On the left side are presented phenomena related to ionisation by precipitating protons, subionospheric radio wave propagation and catalytic reaction cycles of the HO_x and NO_x gases. Also shown are the altitudes regions where the cycles are effective (as indicated by the curly brackets). On the right are shown phenomena related to dynamics. The approximate location of the polar night jet is presented as red circle and the darker colour indicates the area where the peak winds are observed. The red curve depicts the approximate location of the polar vortex. Location of latitudes 45° and 60° are indicated with the respective numbers (taken from Seppälä, 2007).

Figure 9. Combined observations of NO_2 during the Northern Hemisphere winter 2003 – 2004, showing (top) the >10 MeV GOES-11 proton flux $cm^{-2}s^{-1}sr^{-1}$ (heavy line) and K_p index (light line), (middle) high-altitude ionisation levels determined

from the subionospheric radio wave index, and (bottom) GOMOS nighttime and POAM III daytime (SS) NO_2 mixing ratios, with the POAM data shown inside heavy boxes. Both data sets have been zonally averaged over 2 days. Note the differing colour scales for the two satellite data sets. These observations show the generation and descent of NO_x into the upper stratosphere. From Seppälä et al. (2007b).

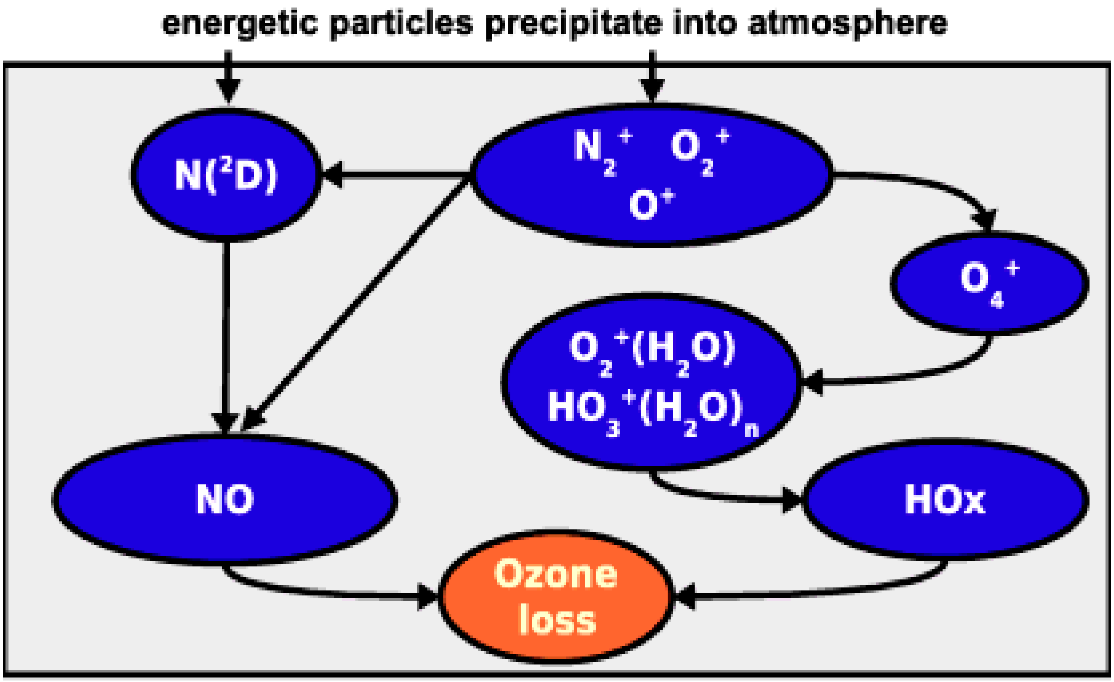

Figure 1. Particle precipitation effects on the ion-chemistry of the atmosphere.

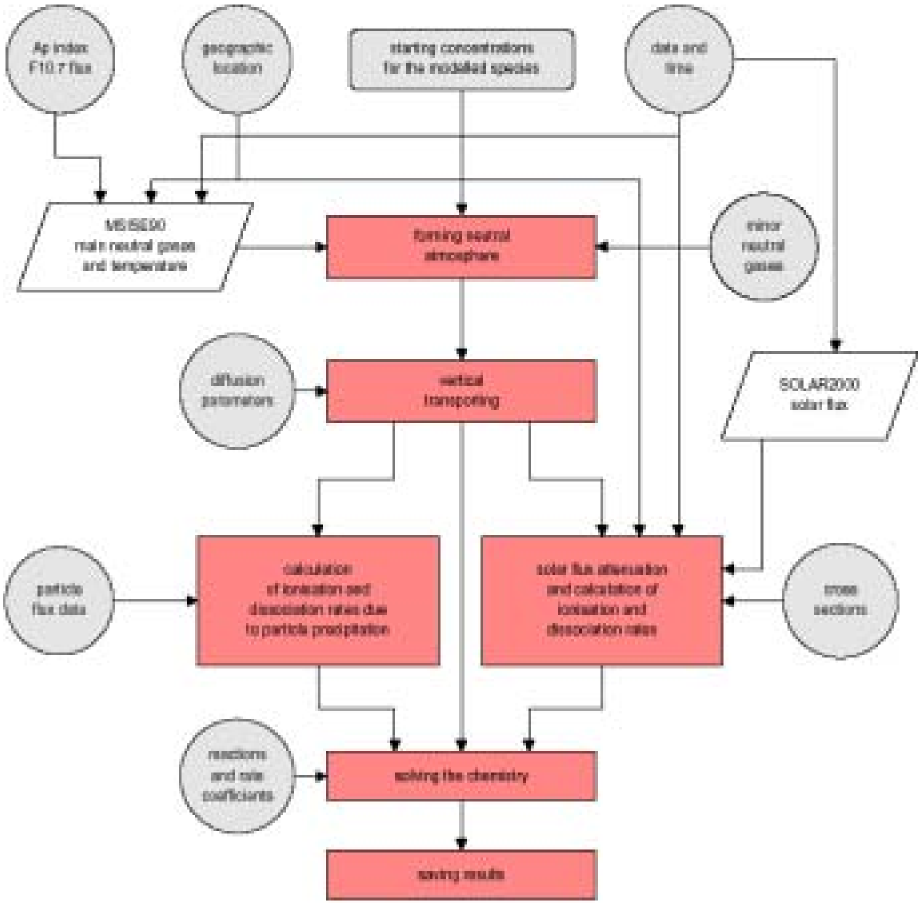

Figure 2. A graphical representation of the SIC model structure. Schematic structure of the Sodankylä Ion and Neutral Chemistry model. The circles, tilted squares, and squares indicate external input, external models used, and modules of the SIC model, respectively (taken from Verronen, Fig 4.1, 2006).

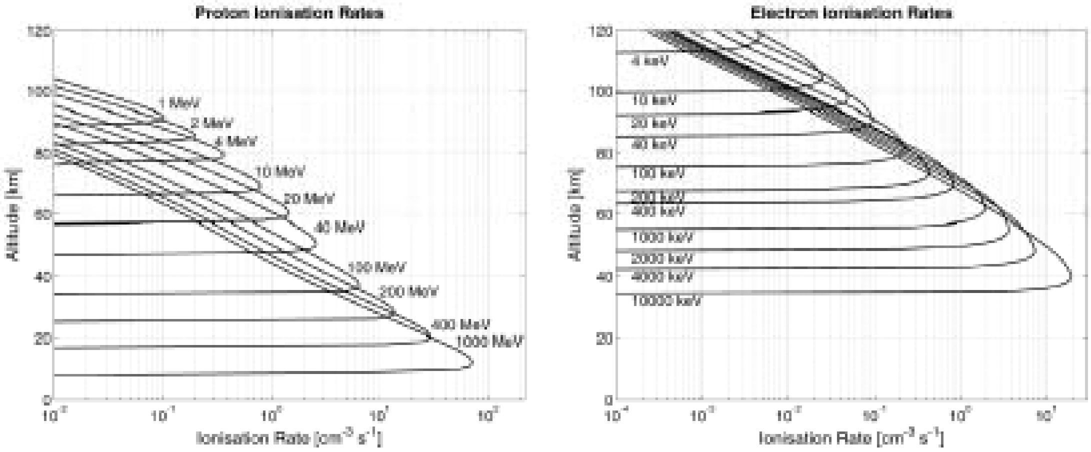

Figure 3. Altitude versus ionisation rates for monoenergetic beams of protons 1-1000 MeV (left) and electrons 4-10000 keV (right).

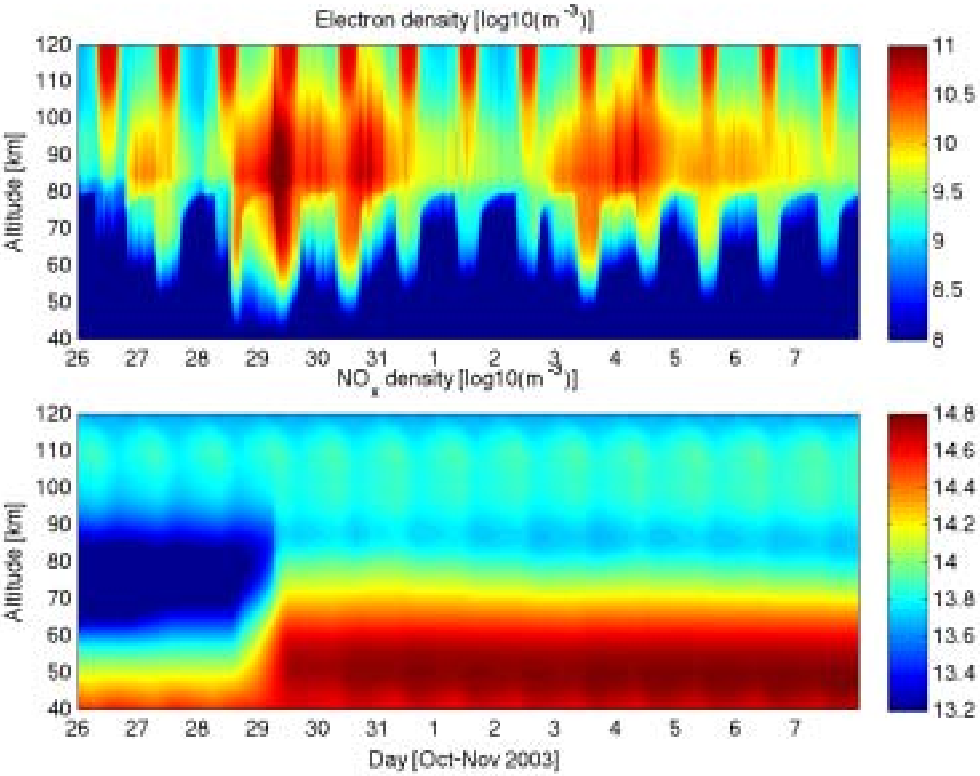

Figure 4. The effect of the Halloween solar proton events on electron number density and NO_x as modelled by SIC at 70° N latitude, 0° longitude. The simulated electron number density ($\log(m^{-3})$), from 40-120 km altitude, with time is shown in the upper panel, and the concentration of NO_x ($\log(m^{-3})$) over the same altitude range is shown in the lower panel. Maximum NO_x production occurs at ~50 km altitudes.

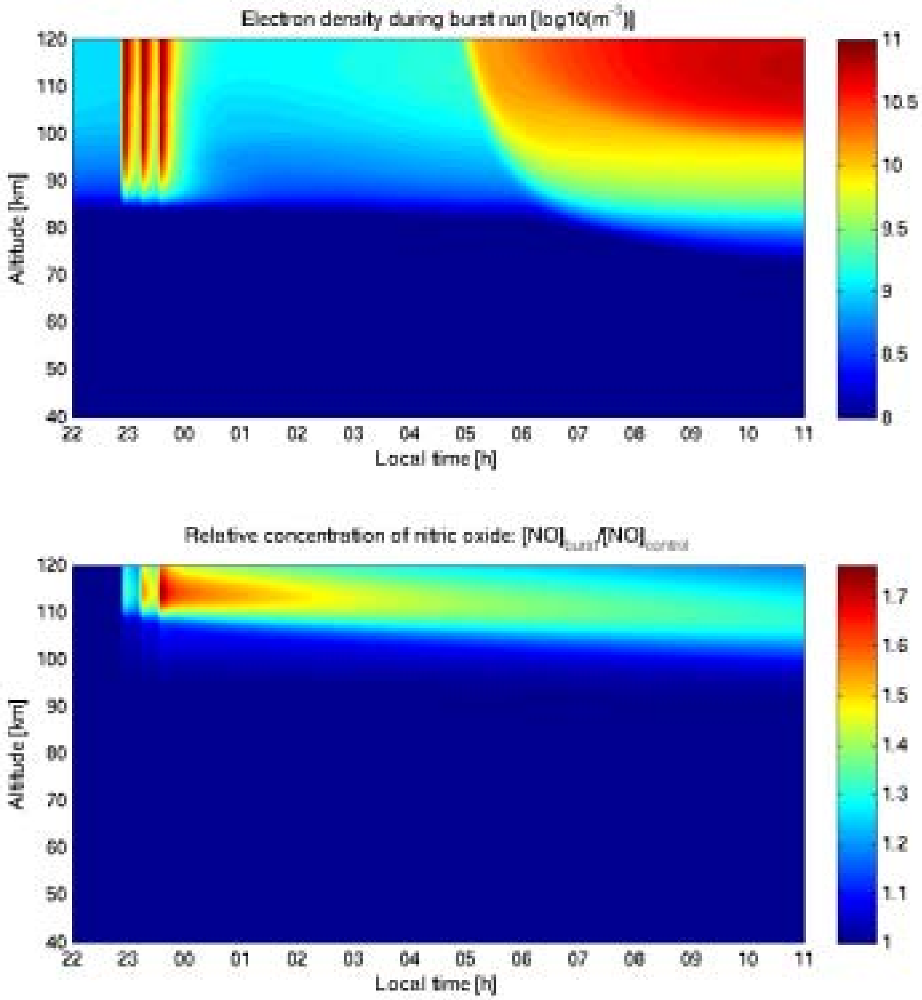

Figure 5. The effect of auroral electron bursts on electron number density and NO concentration. The bursts of electrons have a characteristic energy of 5 keV and a total energy flux of 10 mW m^{-2}. Upper panel: electron number density during the burst run. Lower panel: the behaviour of NO concentration relative to the background level, i.e., the result of the burst run divided by the result of the control run. The electron bursts last 5 min each, starting at 23:05, 23:25, and 23:45 LT.

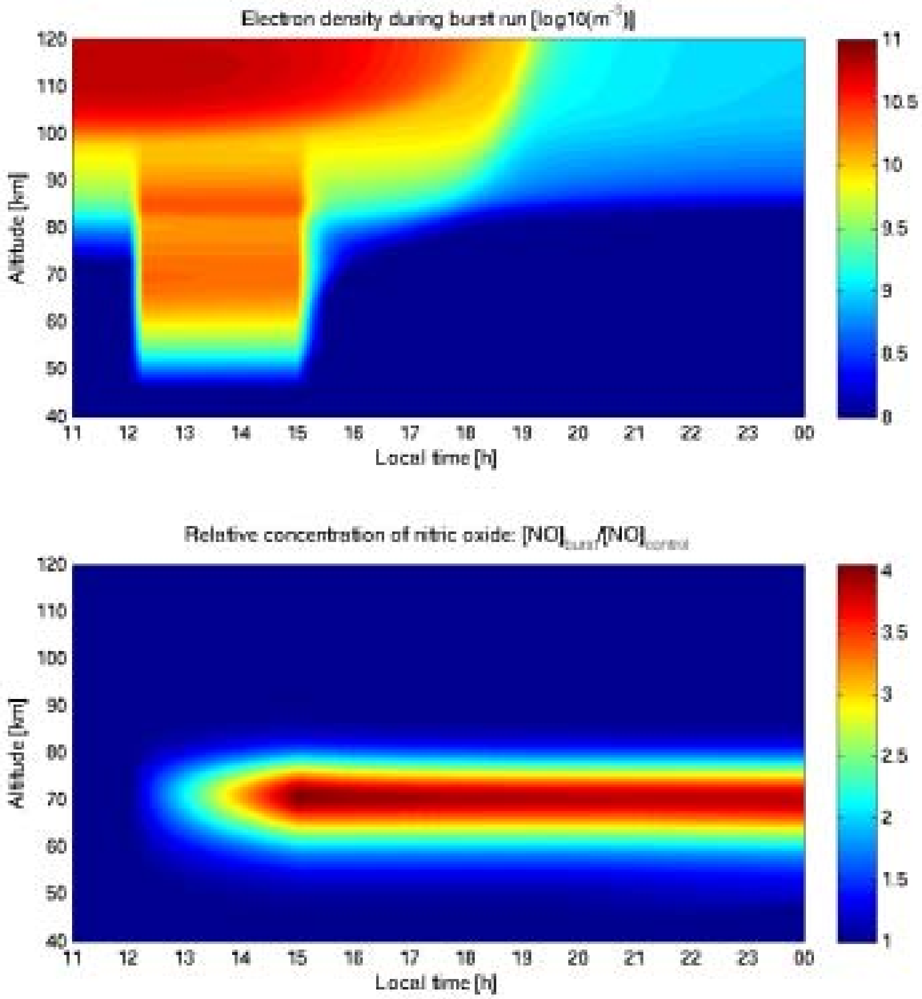

Figure 6. Same as Figure 5, but showing the effect of a 3 hour long burst of REP on electron number density and NO_x levels using the precipitating fluxes measured in the bounce loss cone at *L*=3.5-4 by the UARS on 18 May 1992 (Gaines et al., 1995). The spectrum of the REP event is very hard, containing significant fluxes at energies as high as 5 MeV.

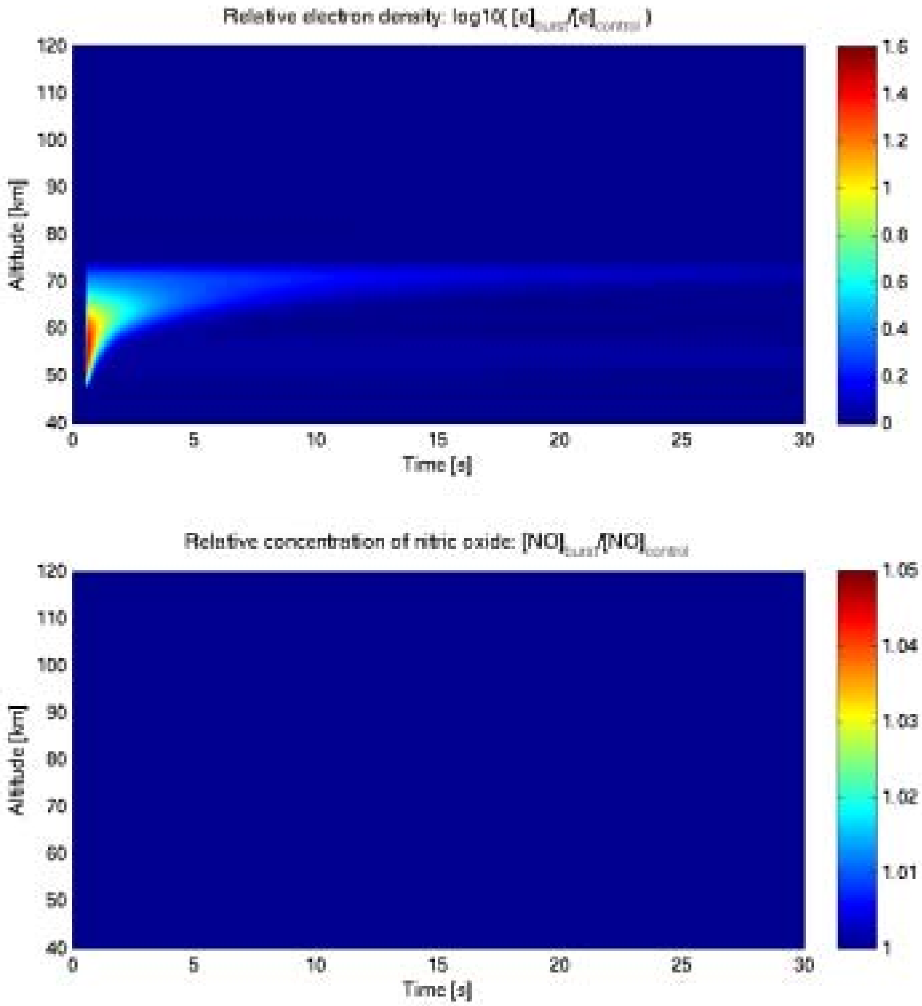

Figure 7. Same as Figure 5, but showing the effect of a REP microburst on electron number density and NO_x levels. We have assumed a 0.1 s burst of 2 MeV monoenergetic relativistic electrons with a flux taken from those reported by SAMPEX.

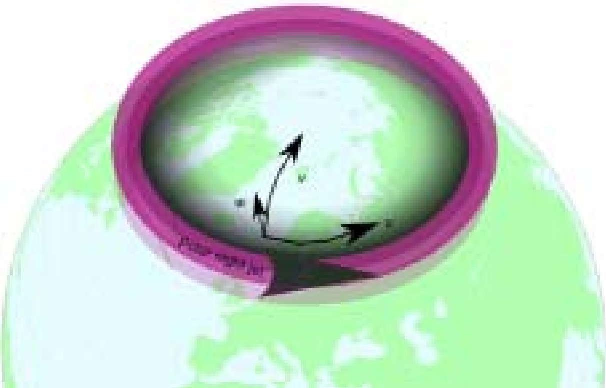

Figure 8a: Approximate location of the Northern Hemisphere Polar Night Jet, inside which the polar vortex is formed, and the wind vector directions (zonal *u*, meridional *v* and vertical *w*).

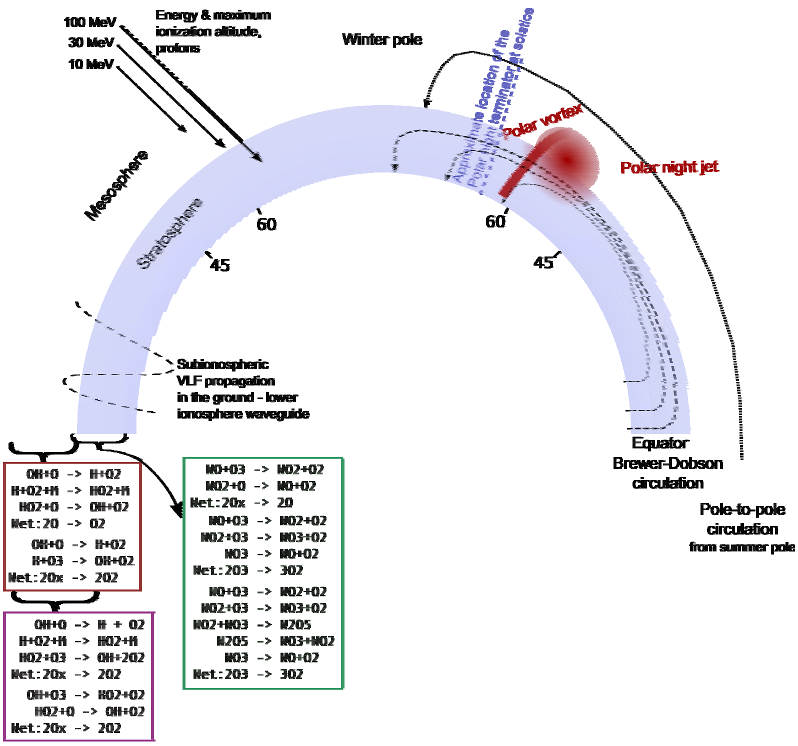

– **8b**: Different phenomena in the winter pole middle atmosphere. On the left side are presented phenomena related to ionisation by precipitating protons, subionospheric radio wave propagation and catalytic reaction cycles of the HO_x and NO_x gases. Also shown are the altitudes regions where the cycles are effective (as indicated by the curly brackets). On the right are shown phenomena related to dynamics. The approximate location of the polar night jet is presented as red circle and the darker colour indicates the area where the peak winds are observed. The red curve depicts the approximate location of the polar vortex. Location of latitudes 45° and 60° are indicated with the respective numbers (taken from Seppälä, 2007).

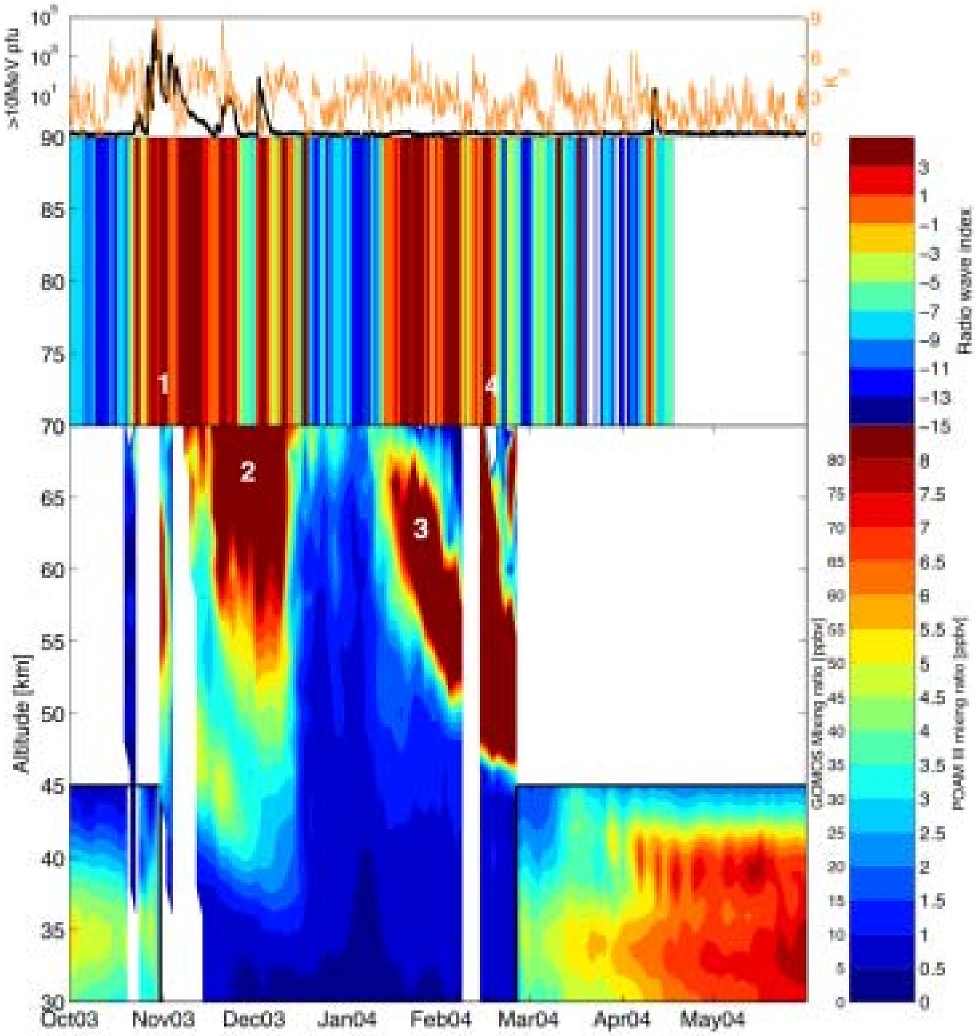

Figure 9. Combined observations of NO_2 during the Northern Hemisphere winter 2003 – 2004, showing (top) the >10 MeV GOES-11 proton flux $cm^{-2}s^{-1}sr^{-1}$ (heavy line) and K_p index (light line), (middle) high-altitude ionisation levels determined from the subionospheric radio wave index, and (bottom) GOMOS nighttime and POAM III daytime (SS) NO_2 mixing ratios, with the POAM data shown inside heavy boxes. Both data sets have been zonally averaged over 2 days. Note the differing colour scales for the two satellite data sets. These observations show the generation and descent of NO_x into the upper stratosphere. From Seppälä et al. (2007b).